Ionics (2022) 28:719–732
https://doi.org/10.1007/s11581-021-04365-7

ORIGINAL PAPER

Modeling and experimental analysis of the thermal and electrochemical characteristics of lithium-ion cells with different electrode thickness

Zhoujian An[1,2] · Yabing Zhao[1,2] · Tianlu Shi[1,2] · Dong Zhang[1,2]

Received: 4 August 2021 / Revised: 1 November 2021 / Accepted: 17 November 2021 / Published online: 25 November 2021

Abstract
The transportation characteristics of Li^+ in the active materials significantly affect the life and overall performance of lithium-ion cells. Analyzing the relationship between electrode thickness and heat/mass-related characteristics is thus very important for lithium-ion cells. The objective of this study was to investigate the effect of electrode thickness on the cell performance by developing a precise one-dimensional electrochemical–thermal coupled model with experimental validation. The thermal and heat-generation characteristics were investigated firstly. Then, the effects of the electrode thickness on the short-term and long-term electrochemical performance of lithium-ion cells were also explored experimentally and numerically from the perspectives of Li^+ transport characteristics and discharging behaviors. The results indicated that the electrode thickness had a significant influence on the cell performance. Firstly, the cell with a thicker electrode showed a lower voltage plateau and an earlier stopping of the discharging process compared with the cell with a thinner electrode during a single discharging test; meanwhile, the cell with a thicker electrode presented a faster capacity degradation rate in the long-term cyclic tests. These influences were explained through the Li^+ transportation mechanism and the electrochemical–thermal coupled effect.

Keywords Lithium-ion cell · Electrode thickness · Electrochemical performance · Mechanical stress · Thermal behavior

Introduction

Lithium-ion cells are a preferred power source owing to their performance advantages in many applications, e.g., electronic devices and hybrid or pure electric vehicles [1–3]. Energy density and rate capability have become major concerns for the application of lithium-ion cells. Improving the energy density (Wh/m^3) is effective for saving space in electric vehicles or energy storage power stations while still meeting the energy requirements. From the perspective of electrode structure, increasing the electrode thickness is an effective method for improving the energy density of cells because the proportion of inactive material, namely the separator and current collector, can be reduced using a thicker electrode in the cell [4, 5]. For a pack with a required capacity, a higher energy density of the cell means a smaller amount of cell monomers in the pack. As a result, the complexity of the pack will be simplified, and the package cost of the pack will be reduced. Nevertheless, increasing the electrode thickness adversely affects the rate capability of the cell, i.e., the maximum limited discharge rate, because the transport resistance of Li^+ and electrons in the active material will increase with the thickness of the electrode owing to the lengthened transport distance [6].

The mechanism for the influence of electrode thickness has been extensively studied in previous experimental research [7–9]. For example, Zheng et al. [7] comparatively investigated the power density, energy density, and cyclic charging/discharging behaviors of NCM and $LiFePO_4$ cells with different electrode thicknesses. The results demonstrated that increasing the electrode thickness could significantly improve the energy density of the cell units at the cost of the rate capacity and power density, and the capacity degradation rate would also be accelerated. Hamankiewicz et al. [8] revealed that the thinnest electrodes exhibited the minimum discharge capacity drop when the discharging

✉ Zhoujian An
anzhoujian@lut.edu.cn

1 College of Energy and Power Engineering, Lanzhou University of Technology, Lanzhou 730050, China

2 Key Laboratory of Fluid Machinery and System, Lanzhou 730050, Gansu Province, China

C-rate was increased from 1 to 30C. The Li^+ near the anode/current collector interface will diffuse with a long transport distance in a thicker electrode during the discharging process. This causes an uneven distribution of the Li^+ intercalation/de-intercalation rates across the electrode owing to the greater Li^+ migration behavior in the electrode, particularly for higher discharge rates or discharge at lower operating temperatures, as shown from an inside view [10]. The uneven distribution of the Li^+ reaction rate in the electrode will induce stress in layered electrode plates as a result of violent Li^+ de-intercalation or intercalation reactions in the local region [11, 12].

As mentioned above, the electrode thickness is an important structural parameter for both the performance and cost of cells. However, most previous reports on the performance of cells with different electrode thicknesses have been based on qualitative experimental research, which has only considered the external performance of the cells, e.g., the capacity degradation rate, impedance, and rate capability. Thus, explanations for the Li^+ diffusion characteristics and heat generation mechanism in the electrode with different thicknesses are still lacking owing to the difficulty and complexity of these experiments. The external behaviors and overall performance are closely related to the internal electrochemical performance and thermal behavior in the electrode layer, which induce different electrochemical parameters and stress distributions across the electrode and directly influence the lifespan and safety of cells during long-term operation. The transport limitation of Li^+ is more severe at lower temperatures, and the performance degradation will be more pronounced for cells operating in cold environments [13]. Comprehensive research on electrodes with different thicknesses at different operating temperatures is also essential and valuable for designing high-performance and low-cost electrodes to meet the current application requirements.

Recently, numerical methods have played a significant role in studies on lithium-ion cells [14–17]. For example, Mei et al. established an electrochemical–thermal coupled model, and the effect of electrode design parameters on battery performance was investigated. Also, a multi-parameter and multi-objective optimization procedure was performed via two optimization methods [18]. Compared to experimental investigations, both the electrochemical performance and thermal behavior at the electrode level can be obtained with an electrochemical–thermal coupled model. Thus, numerical methods are effective for revealing the mechanism by which the electrode thickness affects the performance of lithium-ion cells from a microscopic view combined with experiments.

In this study, the influence of electrode thickness on the electrochemical characteristics and thermal behavior, including the capacity degradation rate, internal resistance, and temperature response, was comprehensively analyzed using an electrochemical–thermal coupled model and experimental measurements. The short-term (one time) and long-term performance of cells with different electrode thicknesses were experimentally analyzed, and an explanation was presented from mechanical and thermal perspectives based on the results obtained using the electrochemical–thermal coupled model.

Experimental setup

In the present study, all experiments were conducted with two types of brand-new commercial 18,650 cylindrical $LiFePO_4$ cells with various electrode thicknesses. The capacities of the cells with a thicker electrode (cell-A) and a thinner electrode (cell-B) were 1530 mAh and 1000 mAh, respectively. The specifications and parameters of the different layers of these cells are listed in Table 1. As listed in Table 1, the energy density of the cell with a thicker electrode reached 296 Wh/L, whereas it was only 193 Wh/L for the cell with a thinner electrode, even though both cell-A and cell-B were 18,650-type models. However, the maximum discharge current of cell-B (30C) was ten times larger than that of cell-A (3C).

To decrease the impact of irreversible capacity fading of the brand-new cells during the performance tests, both cells were first cyclically charged/discharged five times to condition the performance at room temperature, which was roughly controlled within 298 ± 2 K by adjusting the air conditioning system. These cycles were conducted for the new cells to format the solid electrolyte interface (SEI). The cells were charged in galvanostatic-potentiostatic mode at a rate of 0.5C, and the cutoff current and voltage were C/20

Table 1 Specifications of cell-A and cell-B

	cell-A	cell-B
Model	18,650 (cylindrical)	18,650 (cylindrical)
Rated capacity (mAh)	1530	1000
Rated voltage (V)	3.2	3.2
Weight (g)	40 ± 2	39.4 ± 1
Energy density of the cells (Wh/L)	296	193
Specific energy of the cells (Wh/kg)	122.4	81.2
Maximum discharge current (C)	3	30
Maximum charge current (C)	1	1.5
Thickness of Cu foil (μm)	9	9
Thickness of the anodic layer (μm)	59	29.5
Thickness of the separator (μm)	20	20
Thickness of the cathodic layer (μm)	92	46
Thickness of Al foil (μm)	16	16

and 3.65 V, respectively. Correspondingly, the discharging process was performed in galvanostatic mode with a cutoff voltage of 2 V.

Subsequently, both conditioned cells were galvanostatically discharged at 1C, 2C, and 3C with an identical initial temperature (298 ± 2 K) under adiabatic conditions by wrapping the cells with glass fiber which can effectively guarantee that the thermal conditions for the cells discharged with specified rate were the same and avoided being affected by operating temperature; the initial temperatures of the cells were the same as the ambient temperature during the different discharging processes. Five thermocouples were uniformly placed on the surface of the cells along the axial direction to measure the temperature variation of the cells during the discharge process. The voltage–capacity curve and resistance were also recorded during the discharging process.

The effect of the electrode thickness is also embodied in the capacity degradation rate during long-term cycling. The other group of conditioned cells was cyclically charged/discharged to obtain the capacity degradation rate during cycling. Both cell-A and cell-B were cyclically charged in galvanostatic-potentiostatic mode (0.5C) and discharged in galvanostatic mode (1C) with cutoff voltages of 3.65 V and 2 V, respectively, for 100 cycles. The cutoff current was C/20 for the charging process. During these processes, the discharging voltage curves and capacity of each cycle were recorded to analyze the influence of the electrode thickness on the long-term cyclic performance of lithium-ion batteries. For all tests, a 34970A data acquisition device was used to acquire and record the temperature data, while the voltage, capacity, and internal resistance of the cells were synchronously recorded using a Neware battery charging/discharging instrument (BTS-60V100A).

Mathematical model and validation

A lithium-ion battery is laminated and composed of multilayer cells in parallel, and each cell is a complete charging and discharging unit. Therefore, to study the electrochemical characteristics and thermal behavior in electrode layers with different thicknesses, the electrochemical–thermal coupled model can be simplified as a one-dimensional (1D) model because the Li^+ diffusion is mainly concentrated in the direction perpendicular to the layer structure. A schematic of the 1D computational domain is shown in Fig. 1. The computational domain includes an anode current collector, anode, separator, cathode, and cathode current collector. The active electrode material in the cathode was $LiFePO_4$, and graphite (C_6) was used as the anode. The separator of the cell unit was a porous polymer membrane, which was used to separate the cathode and anode layers. The pores of the electrode layers and separator were filled with electrolyte to provide a passageway for Li^+ diffusion and transfer. A $LiPF_6$ solution with a concentration of 1500 mol/m^3 was employed as the electrolyte in the present model, in which the solvent was a mixture of dimethyl carbonate (DMC) and ethylene carbonate (EC) with a volume ratio of 1:2.

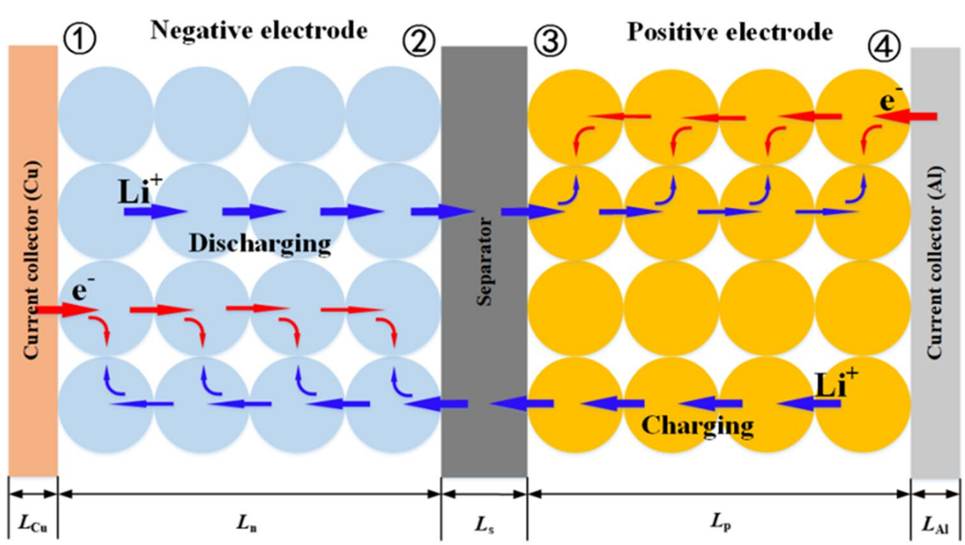

Positive electrode $$Li_aFePO_4 \underset{discharge}{\overset{charge}{\rightleftharpoons}} Li_{a-c}FePO_4 + cLi^+ + ce^-$$

Negative electrode $$Li_bC_6 \underset{charge}{\overset{discharge}{\rightleftharpoons}} Li_{b-c}C_6 + cLi^+ + ce^-$$

Fig. 1 Schematic of the 1D cell unit

The 1D electrochemical–thermal coupled model was established based on the porous electrode theory proposed by Newman et al. [19] and the heat generation model developed by Rao et al. [20] following the principles of mass conservation, charge conservation, electrochemical kinetics, and energy balance.

Governing equations and parameters

As mentioned above, the electrochemical–thermal coupled model was built based on mass conservation, charge conservation, electrochemical kinetics, and energy balance. The diffusion of Li^+ in the active electrode material is controlled by Fick's law, and it is determined from both Fick's law and concentrated solution theory in the electrolyte. Similarly, the charge conservation in the solid phase is governed by Ohm's law. The current in the electrolyte includes two items: the current resulting from Li^+ transfer dominated by Ohm's law and the current generated by Li^+ diffusion governed by the concentration gradient. The electrochemical reaction occurs at the interface of the electrode material particles and electrolyte along with Li^+ intercalation or de-intercalation, which is determined by electrochemical kinetics. The heat source items in the energy conservation equation include ohmic heat, polarization heat, and the reversible entropy change during the charging and discharging processes. The governing equations are listed in Table 2.

Table 2 Conservation equations for the 1D electrochemical–thermal coupled model

Physics	Equations	
Charge conservation	$i_s = -\sigma_s^{eff} \frac{\partial \varphi_s}{\partial x}; \sigma_s^{eff} = \sigma_s \varepsilon_s^{\gamma_s}$	(1)
	$i_l = -\sigma_l^{eff} \frac{\partial \varphi_l}{\partial x} + \frac{2RT\sigma_l^{eff}}{F}\left(1 + \frac{\partial \ln f_\pm}{\partial \ln c_l}\right)(1 - t_+)\frac{\partial \ln c_l}{\partial x}; \sigma_l^{eff} = \sigma_l \varepsilon_l^{\gamma_l}$	(2)
	$K_{junc} = \frac{2RT}{F}\left(1 + \frac{\partial \ln f_\pm}{\partial \ln c_l}\right)(1 - t_+) = \frac{2RT}{F}\nu$	(3)
Mass conservation	$\frac{\partial c_s}{\partial t} + \frac{1}{r^2}\frac{\partial}{\partial r}\left(-r^2 D_s \frac{\partial c_s}{\partial r}\right) = 0$	(4)
	$\varepsilon_l \frac{\partial c_l}{\partial t} + \frac{\partial}{\partial x}\left(-D_l^{eff}\frac{\partial c_l}{\partial x}\right) = \frac{S_a j_{loc}}{F}(1 - t_+); D_l^{eff} = D_l \varepsilon_l^{\gamma_l}$	(5)
Electrochemical kinetics at the interface	$j_{loc} = j_0\left\{\exp\left(\frac{\alpha_{a,i}F}{RT}\eta\right) - \exp\left(-\frac{\alpha_{c,i}F}{RT}\eta\right)\right\}$	(6)
	$j_0 = Fk_0 c_l^{\alpha_a}(c_{l,max} - c_{l,surf})^{\alpha_a} c_{l,surf}^{\alpha_c}$	(7)
	$\eta_i = \varphi_s - \varphi_l - U_i$	(8)
Energy conservation	$Q_{rea} = S_a j_{loc} T \frac{\partial U}{\partial T} = S_a j_{loc} T \frac{\Delta S}{F}$	(9)
	$Q_{act} = S_a j_{loc} \eta$	(10)
	$Q_{ohm} = -i_s \cdot \frac{\partial \varphi_s}{\partial x} - i_l \cdot \frac{\partial \varphi_l}{\partial x}$	(11)
	$\rho C_p \frac{\partial T}{\partial t} - k\nabla^2 T = Q_{rea} + Q_{act} + Q_{ohm}$	(12)

The boundary conditions, including the charge conservation, mass conservation, and thermal-related boundary conditions, are listed in Table 3.

The parameters used in the present electrochemical–thermal coupled model include constant parameters and temperature, concentration, and state of charge (SOC)-dependent parameters. In this model, the dependent parameters, including the reaction rate constant, k_0, of the anode and cathode, as shown in Eq. 7, and the Li^+ diffusion coefficient, D_s, in the solid phase, given in Eq. 4, are temperature-dependent parameters following the Arrhenius equations. The open circuit potential, U_i, for the anode and cathode given in Eq. 8 is also a function of SOC and temperature. The concentration in the electrolyte varies across the thickness of the electrode, and it significantly affects the electrical conductivity, σ_l, expressed in Eq. 2; the diffusion coefficient, Dl, described in Eq. 5; and the thermodynamic factor, ν, as shown in Eq. 3. The model parameters have been extensively discussed and are in accordance with previous studies [10, 21] except for the initial SOCs of the anode and cathode, which were modified to 0.8 and 0.13, respectively, in the present study based on the capacity of the cells used [22]. Hence, the other parameters are not repeated here for brevity.

Model validation

The reliability of the model was validated from thermal and electrochemical perspectives by comparing the numerical results with experimental results, as shown in Fig. 2. The electrochemical validation was conducted by plotting the voltage against the depth of discharge (DOD), where a value of 0 represents the fully charged state and 1 is considered fully discharged. It can be seen that the results obtained from the electrochemical–thermal coupled model can basically reflect the voltage and temperature variation during the discharging process at various C-rates. The slight discrepancy between the experimental and simulated results is mainly a result of the assumptions in the model [23]. Overall, this

Table 3 Boundary conditions of the electrochemical–thermal coupled model

Physics	Boundary conditions	
Charge conservation	$\varphi_s\big|_{x=0} = 0; -\sigma_s^{eff}\frac{\partial \varphi_s}{\partial x}\Big|_{x=L_{Cu}+L_n,\ x=L_{Cu}+L_n+L_p+L_{sep}} = 0; -\sigma_s^{eff}\frac{\partial \varphi_e}{\partial x}\Big|_{x=L} = I_{app}; \frac{\partial \varphi_e}{\partial x}\Big|_{x=L_{Cu},\ x=L} = 0$	(13)
Mass conservation	$\frac{\partial c_s}{\partial r}\Big|_{r=0} = 0; D_s\frac{\partial c_s}{\partial r}\Big|_{r=r_p} = -\frac{j_{loc}}{S_a F}; \frac{\partial c_e}{\partial x}\Big|_{x=L_{Cu},\ x=L_{Cu}+L_n+L_s+L_p} = 0$	(14)
Energy conservation	$-k\frac{\partial T}{\partial n} = h(T - T_{amb})$	(15)

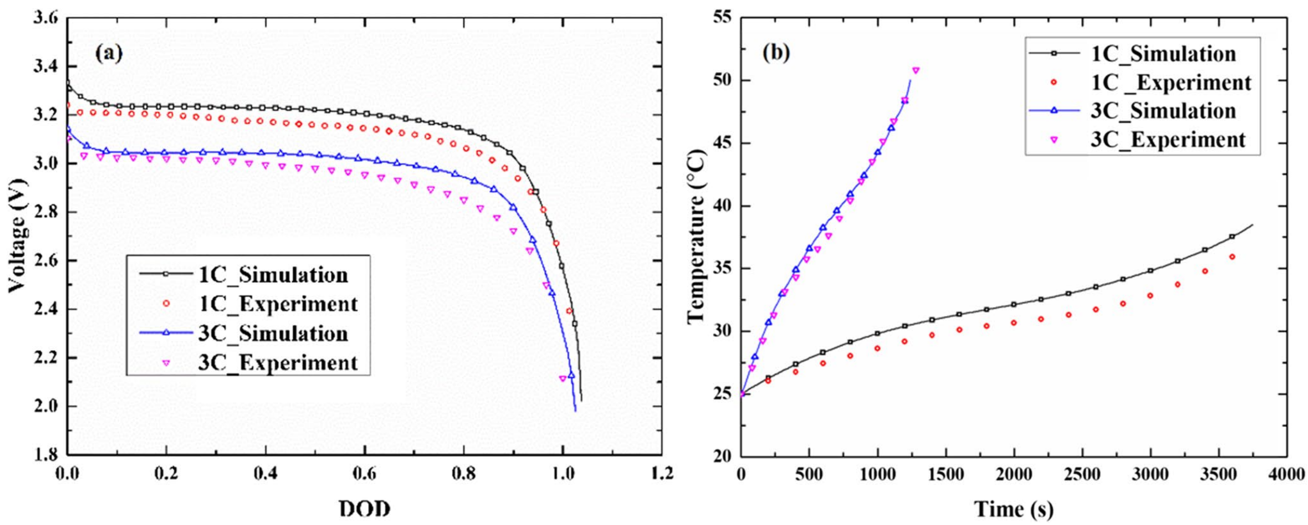

Fig. 2 Model validation of the **a** electrochemical performance and **b** thermal performance

coupled model is accurate for simulating the electrochemical and thermal behaviors of lithium-ion cells.

Results and discussion

The electrode thickness plays a significant role in the electrochemical characteristics and thermal behavior of lithium-ion cells for both the one-time discharging process and long-term charging-discharging cycles at both regular and low operating temperatures. All of these effects are discussed in more detail in the following sections.

Short-term performance of cells with various electrode thicknesses

Typical discharging curves for cell-A and cell-B at discharge rates of 1C, 2C, and 3C are shown in Fig. 3. As shown, the voltage plateau strongly depended on the electrode thickness. At the same discharge rate, the voltage of the cell with a thicker electrode (cell-A) was lower than that of the cell with a thinner electrode (cell-B) at the same DOD process. The difference in the voltage plateau between the different cells increased with the discharge rate. The difference in the voltage for cell-A and cell-B was approximately 0.04 V at a discharge rate of 1C, as shown in Fig. 3a; this value reached 0.2 V at 3C, as shown in Fig. 3c. Meanwhile, the discharging capacity of cell-A did not reach the normal capacity provided by the manufacturer, i.e., the normalized capacity was less than 1. However, the normalized capacity of cell-B reached 1 at all discharge rates. This difference can be explained by the fact that the same cutoff voltage (2 V) was used as the stopping condition for both cell-A and cell-B, but the discharging voltage of cell-A was lower than that of cell-B. Therefore, cell-A reached the cutoff voltage earlier than cell-B owing to its lower discharge voltage plateau.

The lower discharge voltage plateau of the cell with a thicker electrode compared with the cell having a thinner electrode at the same C-rate resulted from the polarization effect induced by the internal resistance. The cathode material used in both cell-A and cell-B was $LiFePO_4$, and they had the same open circuit potential. According to Ohm's law, $\Delta U = IR$, the voltage loss is determined by two aspects: internal resistance and applied current density. As listed in Table 4, the internal resistances of cell-A and cell-B were approximately 41.4–46.1 mΩ and 20.9–21.6 mΩ, respectively, at different discharge rates. This higher resistance of the cell with a thicker electrode can be attributed to the longer Li^+ diffusion pathway in the electrode. Simultaneously, the applied current density in the separator, that is current resulted from the ions flow (Li^+) in separator per unit area, increased with a greater thickness of the electrode at the same discharge rate. As a result, the voltage loss of the cell with a thicker electrode was larger than that of the cell with a thinner electrode, and the voltage difference between cell-A and cell-B also increased with the C-rate, as shown in Fig. 3a–c.

Furthermore, the impact of the electrode thickness on the distribution of electrochemical characteristics across the cell unit was also investigated. Electrochemical parameters such as the overpotential, electrolyte potential, and Li^+ concentration distribution in the electrolyte are closely related to the electrochemical performance and thermal behavior of the cell because these parameters are inherent to the polarization effect, electrochemical reaction rate, etc. In particular, the Li^+ concentration distribution across the electrode is intrinsically related to the concentration polarization, which can lead to premature termination of the discharge process;

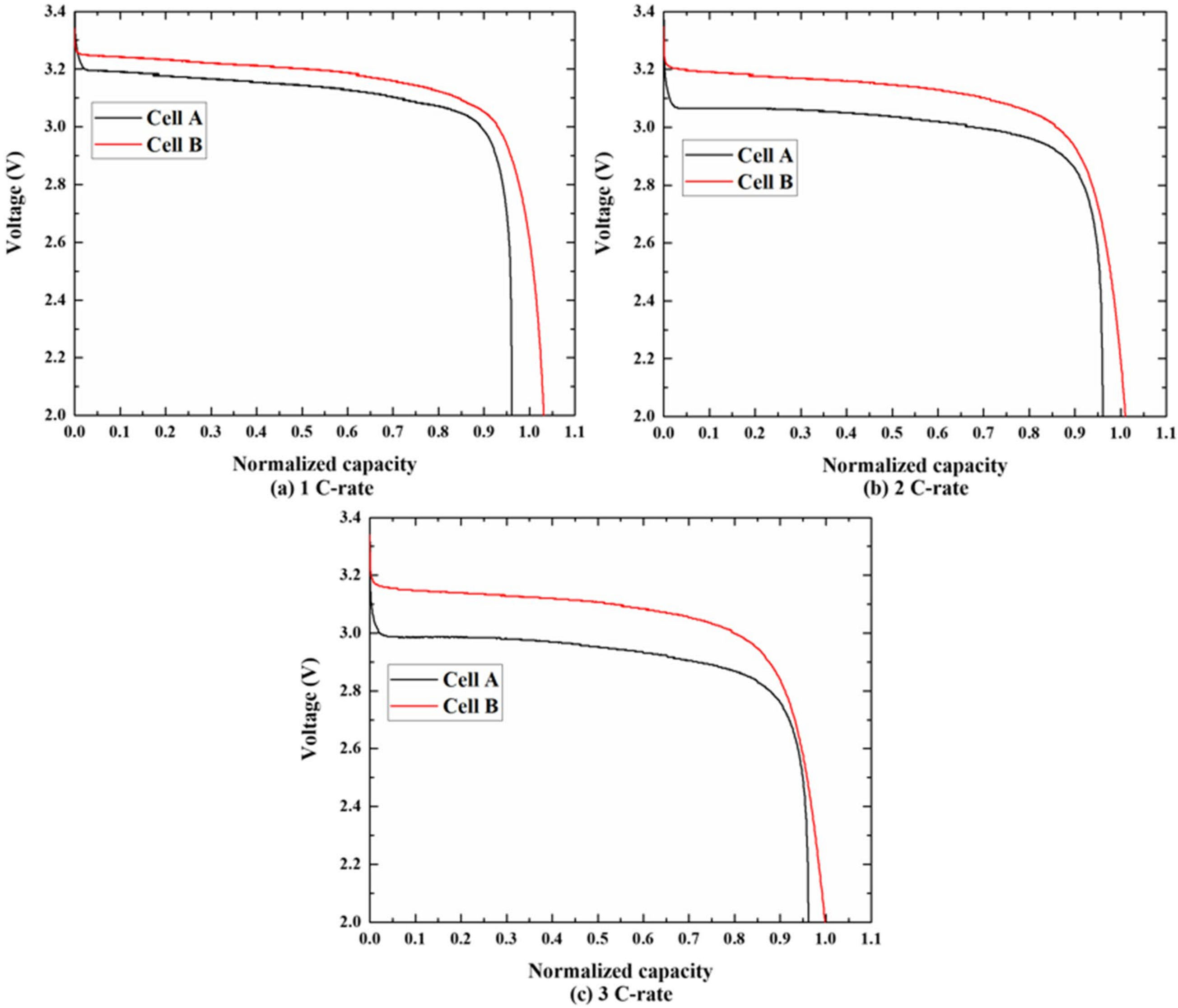

Fig. 3 Experimental discharge curves for cell-A and cell-B

Table 4 Internal resistances of the two cells during the discharging process at different C-rates

Discharge rate	cell-A	cell-B
1C	41.4 mΩ	21.5 mΩ
2C	43.7 mΩ	20.9 mΩ
3C	46.1 mΩ	21.6 mΩ

therefore, it is often recognized as an important contributor to the performance degradation of lithium-ion cells.

The electrolyte Li^+ concentration distribution was considered in the present study based on the electrochemical model, and the normalized electrode width was used for the electrodes with different thicknesses. As depicted in Fig. 4, the Li^+ concentration gradient in the cell unit with a thicker electrode was significantly larger than that in the thinner electrode. For example, the Li^+ concentration difference across the cell unit was 40 mol/m^3 for the thinner electrode at 1200 s. However, this value reached 220 mol/m^3 for the thicker electrode, which represents a higher concentration polarization in the electrode. In addition, an almost unchanged electrolyte potential across the thinner electrode was observed in Ref. [24]. The current in the electrolyte includes two terms, namely the diffusion current and transference current, which follow Fick's law and Ohm's law, respectively. The driving forces of these two terms are the electrolyte concentration gradient and potential difference, respectively. As analyzed above, the applied current density increased with the electrode thickness for the two cells despite discharging at the same C-rate. As a result, the potential

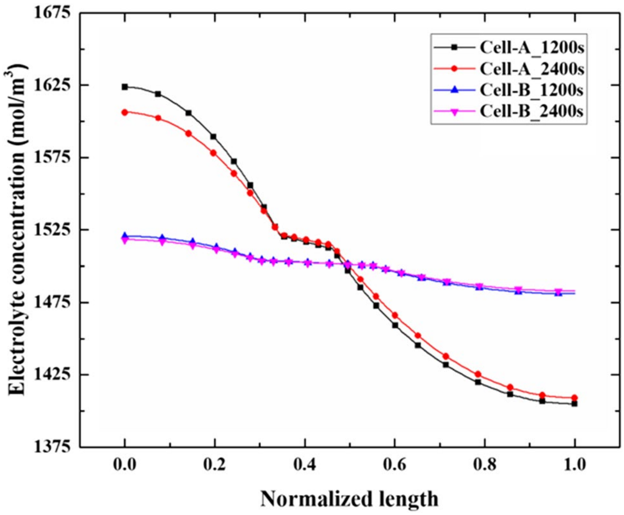

Fig. 4 Comparison of liquid phase Li^+ concentration distributions

gradient and Li^+ concentration gradient in the electrolyte also increased. This higher gradient indicates a stronger polarization effect in the cells and accelerates the capacity degradation.

In summary, the influence of electrode thickness on the short-term electrochemical characteristics of cells was mainly manifested in the lower voltage plateau and discharging capacity for the cell with a thicker electrode owing to the higher internal resistance and applied current density. It also exhibited a strong concentration polarization in the electrolyte, which will ultimately affect the capacity degradation rate of the cell.

Effect of electrode thickness on the long-term performance of cells

To investigate the long-term operating performance (capacity degradation rate) of cells with different electrode thicknesses, both cells were charged and discharged cyclically 100 times at room temperature. Figure 5 shows the discharging curves at the 1st, 50th, and 100th cycles for the two cells. It was found that the voltage–capacity curves were detached for the cell with a thicker electrode at the given cycles, especially in the later period of the discharging process. As the number of cycles increased, the discharging process stopped prematurely. Although the capacity–voltage curves overlapped during the initial process, the cell with the thicker electrode showed a faster capacity degradation rate compared with the discharge curves for the cell with a thinner electrode, as shown in Fig. 5b, which almost overlapped at the given cycle numbers. The negligible difference between the discharging curves for the given cycles indicate a stable electrochemical reaction during the discharging process and a lower active material aging rate in the thinner electrode.

The capacity degradation rates of these two cells in the long-term charging/discharging cyclic tests at room temperature are depicted in Fig. 6, and the results are consistent with the discharge curves in Fig. 5. The cell with a thicker electrode showed a faster capacity degradation rate than the cell with a thinner electrode. The degradation rate was almost linear with the increase in cycle number for cell-A, with a value of 0.4 mAh per cycle within the 100 cycles. However, the capacity of cell-B remained approximately constant during the cyclic process. It can also be deduced that the capacity degradation rate of the thick electrode cell

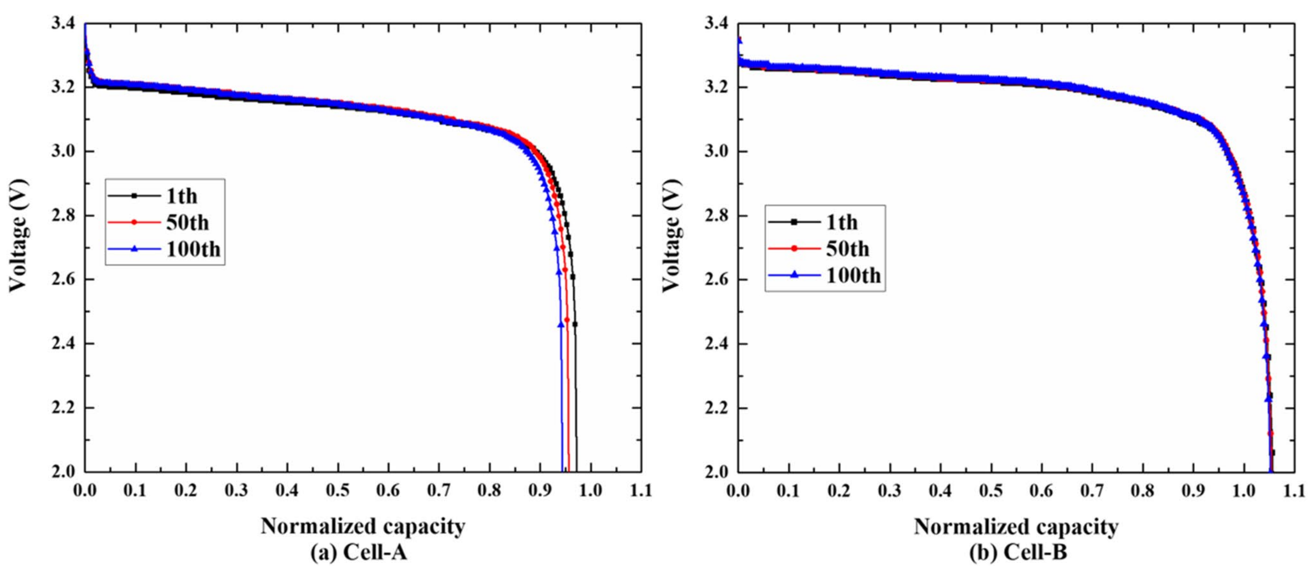

Fig. 5 Experimental capacity–voltage curves for cells with different electrode thicknesses at given cycle numbers

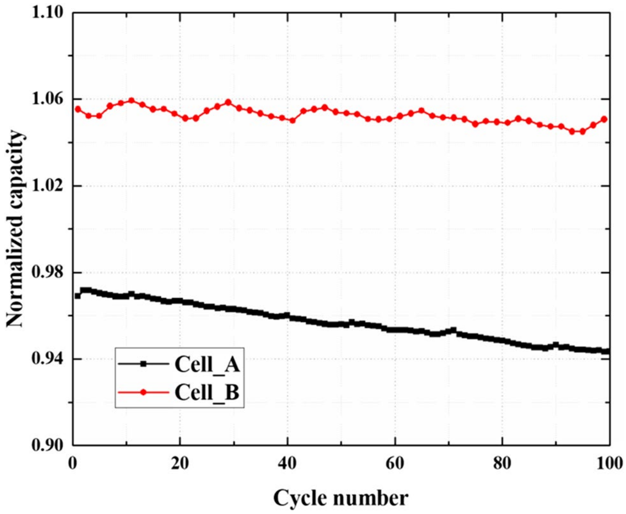

Fig. 6 Experimental capacity degradations curves for cells with different electrode thickness

would further increase with the discharge rate, as indicated by the results reported by Zhao et al. [24] for a Li_2MnO_4 cell. The differences in the capacity rates of these two cells with different electrode thicknesses were analyzed in detail based on a numerical method from an electrochemical perspective.

To investigate the mechanisms of the different voltage and capacity degradation rates of the two cells, the corresponding electrochemical processes were simulated by combining the experimental and electrochemical–thermal coupled model from both mechanical and thermal perspectives.

As a vital indicator of the C-rate and the uniformity of the lithiation or delithiation reactions inside the lithium-ion cell, the local current density on the particle surfaces of the electrode material at a discharge rate of 1C are shown along the thickness direction of the electrochemical cell unit in Fig. 7. The local current density distribution across the cell exhibited obvious differences between cell-A and cell-B. Cell-A exhibited drastic fluctuations and variation at the assigned

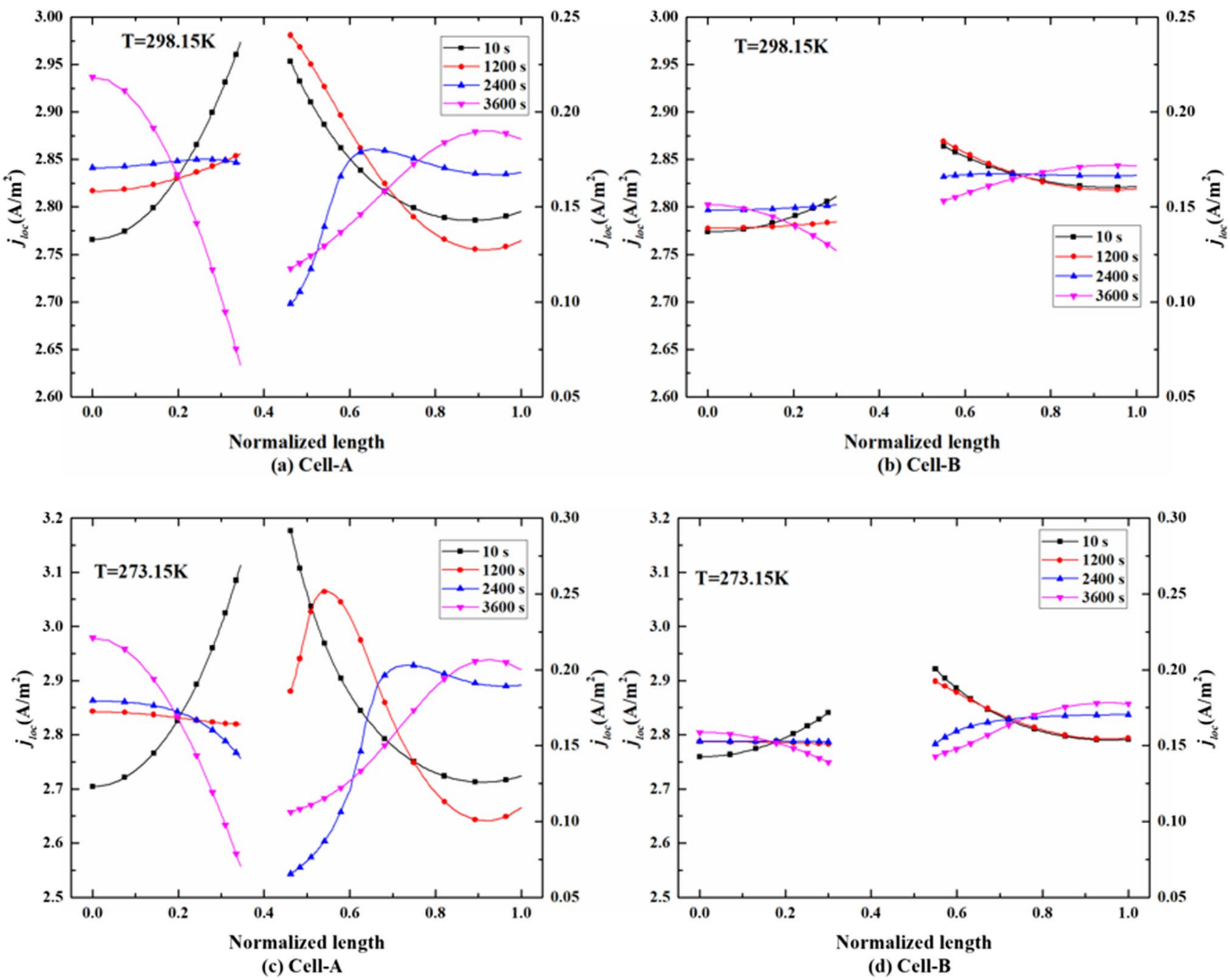

Fig. 7 Comparison of local current densities for cells with different electrode thicknesses and operating temperatures

time during the discharging process. However, the current density distribution was almost flat and showed no variations for cell-B. It was found that the electrochemical reaction rate at the electrode/separator interface increased drastically at the initial stage, and then the peak value of the local current density shifted from the electrode/separator interface to the electrode/current interface for cell-A. Compared with cell-A, although the local current density showed a similar profile for cell-B, the fluctuation was very small and almost flat.

The uneven local current density also led to a fluctuating distribution of the solid-phase Li concentration. Figure 8 shows the superficial Li^+ concentration of the active electrode material particles across the electrode thickness. With a greater thickness of the electrode, the solid-phase Li^+ concentration distribution across the electrode became uneven, as shown in Fig. 8a. This indicates that the depth of the lithiation reaction in the cathode was different, and the active electrode material particles across the electrode layers were not fully and uniformly utilized, especially for the cathode; thus, eventually the Li^+ concentration became unevenly distributed. However, this non-uniform Li^+ concentration distribution would increase and cause premature termination of the discharge process at higher C-rates [24]. Comparatively, the solid-phase Li concentration distribution across the thinner electrode was almost uniform, as shown in Fig. 8b. The other problem that needs to be emphasized and explained is that Li concentration of anode was even compared to the cathode as showed in Fig. 8. This characteristic mainly resulted from two aspects: Li diffusion coefficient in anode was larger than that in cathode and the thickness of anode was thinner than cathode [10]. Both of the two terms determined that the diffusion resistance of Li in anode was smaller than that of cathode and showed a more even distribution. This also proves from the other aspect that thinner thickness could effectively improve the uniformity of electrochemical parameters distribution across electrode.

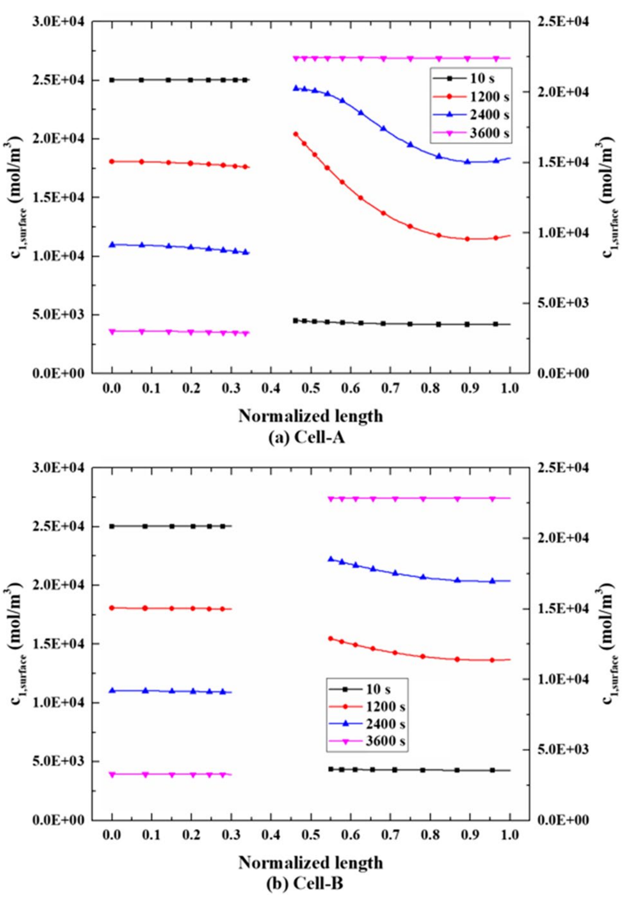

Fig. 8 Li^+ concentrations at the particle surfaces during 1C discharge

This non-uniformity of the local current density in the thicker cell resulted from two aspects: (i) a larger Li^+ flow rate at the electrode/separator interface for the thicker electrode and (ii) a longer Li^+ diffusion distance when intercalating and de-intercalating the electrode.

The internal structure of a cylindrical cell is spiral-wound by the rectangular cell unit [25]. The applied current density in the cell depends on the thickness of the electrode. For an electrode plate with a certain electrode thickness, the applied current density is specific for a given discharge rate, and it increases with the electrode thickness. The Li^+ de-intercalating from the anode will flow through the separator and intercalate in the cathode during the discharging process. The discharging mode used in the present simulation and experiments was the constant-current mode. The quantity of Li^+ participating in the lithiation reaction at the interface of the electrolyte and active material particles was steady at any time during the discharging process and was proportional to the applied current density, i.e., the electrode thickness. For the cell with a thicker electrode, the quantity of Li^+ was much larger than that in the cell with a thinner electrode at the same C-rate. However, as mentioned above (aspect ii), the Li^+ diffusion distance in the cell with a thicker electrode was longer than that of the thinner electrode, resulting in a larger resistance. As a result, most of the Li^+ reacts with the cathode active material particles close to the cathode/separator interface to maintain charge balance at the beginning of the discharging process. As discharging progresses, the degree of lithiation of these particles increases, and the lithiation reaction becomes more difficult. The kinetically favored cathode active material particles in the region close to the separator intercalate more Li^+ than the particles close to the current collector; as a result, the remaining incoming Li^+ needs to diffuse through longer pathways to the deeper regions of the electrode, and the peak of the lithiation reaction rate will move forward to the cathode/current collector interface. This uneven distribution characteristic of the lithiation reaction rate is more severe at higher C-rates and lower operating temperatures [10]. However, for the cell with a thinner electrode, the amount of Li^+ was less and the diffusion distance was shorter, and thus the local current was more uniform across the electrode compared with the thicker electrode. Similarly, the non-uniformity of the local current density dramatically increased with a reduction in the operating temperature for the electrodes at the same C-rate, as depicted in Fig. 7a and c. This non-uniformity resulting from the low temperature was also mitigated by the decrease in electrode thickness, as shown in Fig. 7c and d. It means that temperature and electrode thickness showed a coupling effect on the electrochemical characteristics of lithium-ion battery. That is to say that lower temperature would deteriorate the uniformity of electrochemical reaction rate in the electrode; however, this non-uniformity resulting from the lower temperature would be alleviated by decreasing the electrode thickness. It can be proved that the fluctuation of the local current density of cell-B was much smaller than that of cell-A, although both cells were operating at a lower temperature of 273.15 K as showed in Fig. 7c and d.

Based on the above analysis, the faster degradation rate for the thicker electrode cell could be explained on two levels: the electrode material particle level and the electrode layer level. First, despite charging/discharging at the same rate, the particles in the thicker electrode always undergo a higher Li^+ intercalation/de-intercalation intensity owing to the uneven local current density compared with the thinner electrode. This higher Li^+ intercalation/de-intercalation intensity will more easily lead to particle cracking, SEI growth, and Li^+ plating, and eventually accelerate the degradation rate [26, 27]. Second, as Li^+ continuously intercalates into the cathode layers, the lithiation region in the cathode tends to expand; however, the delithiation regions in the cathode and the current collector remain unformed. Therefore, as shown in Fig. 9, compressive stress was induced in the electrode layer because of the constraint of the current collector; in contrast, tensile stress was induced in the aluminum foil owing to the traction of the electrode layers [11]. The stress in the electrode layer during the galvanostatic discharging process mainly depends on the Li^+ concentration distribution. The region with a larger lithiation degree corresponds to a higher stress level [11]. Therefore, this stress will be aggravated in the thicker electrode owing to the more uneven distribution of the Li^+ concentration, as shown in Fig. 8a. In addition, the peak stress in the electrode will move from the separator/cathode interface to the cathode/current collector interface as the discharge progresses, resulting in an uneven stress distribution in the cathode. These uneven Li^+ intercalation intensities and stress distributions give rise to mechanical failures of electrodes, cracking of active material particles, the loss of lithium inventory, and the loss of active material [28, 29]. This results in different types of degradation of lithium-ion cells, such as an increase in impedance and resistance or loss of capacity and cycle life [30, 31].

During long-term operation, diffusion-induced stress results from the uneven distribution of the solid Li^+ concentration, and local current density is an important factors affecting the degradation rate of lithium-ion cells; this effect is more severe for thicker electrode cells operating at higher charging/discharging rates and lower temperatures [32, 33].

The electrode thickness also affects the thermal behavior of the cell because the electrode thickness is directly associated with the ohmic resistance and the fraction of electrode material within the cell. The experimental temperature variations in the two cells discharged at different C-rates are shown in Fig. 10. Although the discharging time of cell-B was larger than the standard time, i.e. 3600/C-rate seconds, only the temperature variation in the standard time is plotted in Fig. 10, as this is more convenient for comparing the thermal performance of the two cells. It is shown that the temperature variations of cell-A and cell-B with different electrode thicknesses exhibited obvious differences during the discharging process. In general, the temperature of the cell with a thicker electrode was higher than that with a thinner electrode. For example, the temperature of cell-A reached 31.3 °C, whereas it was only 29.9 °C for cell-B when the discharging process terminated, although the discharge time of cell-B was longer than that of cell-A. This difference increased with the C-rate, as shown in Fig. 10.

The heat generation in a cell includes three parts: electrochemical heat, ohmic heat, and polarization heat [10]. Both cell-A and cell-B were model 18,650, and the capacities were 1530 mAh and 1000 mAh, respectively. This higher energy density meant a much higher volume proportion of electrode material in the cell. All three types of heat existed in the active electrode material (anode and cathode), but only ohmic heat was generated in the separator and current collectors. As presented in Ref. [10], the electrochemical reaction and polarization heat dominated the heat generation of the cell, especially at lower discharge rates. There were positive correlations between these two types of heat generation and the volume of electrode material because the generation rates (W/m^3) of these two types of heat were almost equal. Therefore, the electrochemical reaction heat and polarization heat in cell-A were higher than those in cell-B. At the same time, the thickness of the electrode also affects the ohmic heat. In the thicker electrode, according to $Q = I^2R$, the higher ohmic resistance of Li^+ diffusion and transference during the electrochemical reaction process and larger applied current density resulted in a higher ohmic heat generation rate as showed in Fig. 11. For example, the ohmic heat generation rate at the interface between cathode and separator for the cell-A reached to 2250 W/m^3

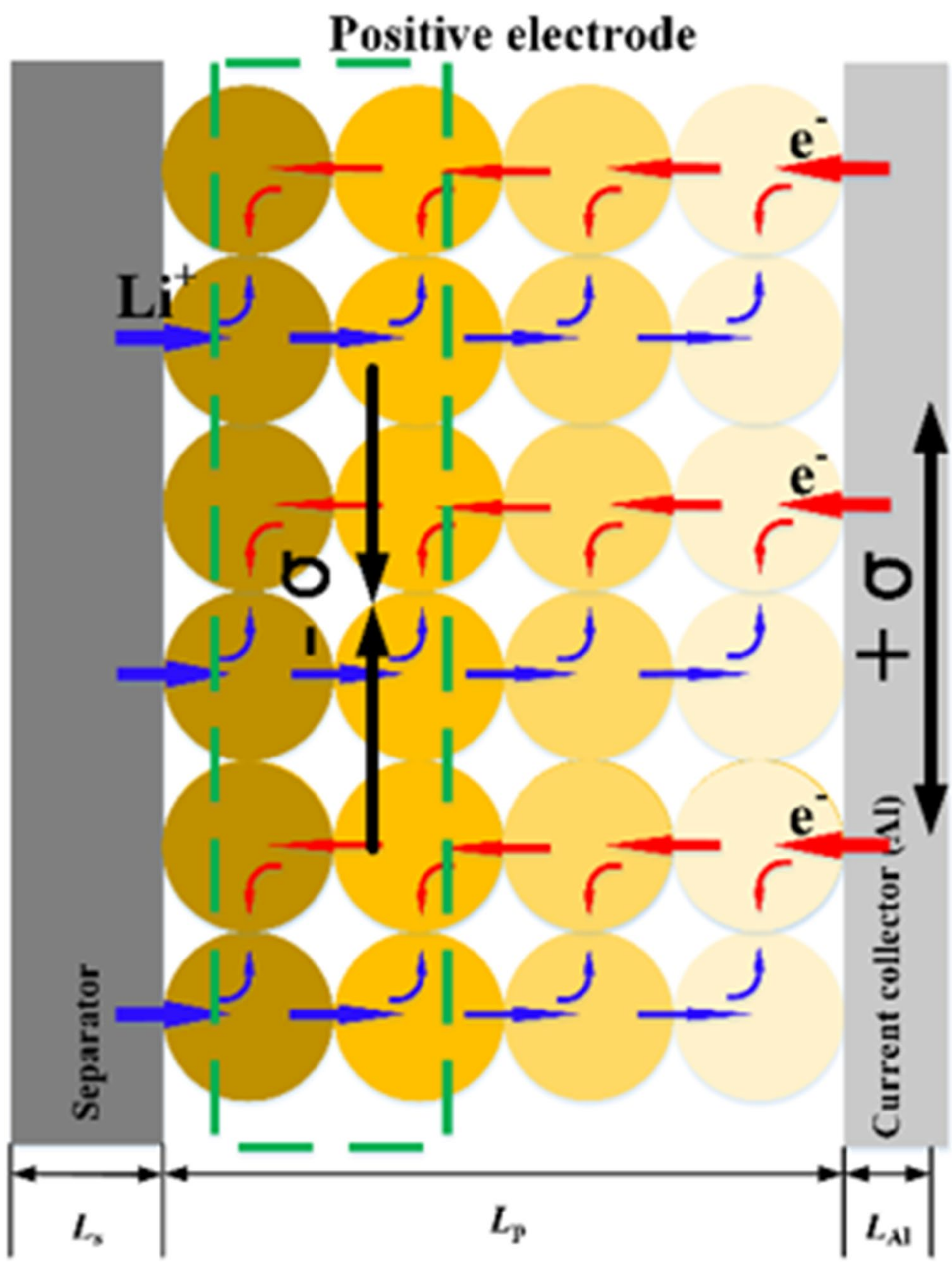

Fig. 9 Schematic of the stress distribution in the cathode (the dark color means a higher lithiation)

compared to that for the cell with thinner electrode, which was only 350 W/m^3. In other words, the maximum of ohmic heat generation rate in thicker cathode was almost six times greater than that in thinner electrode; however, the thickness of electrode was only doubled. As analyzed above, the applied current density was proportional to the thickness of the electrode, which meant that more Li^+ flowed through the electrode and separator in the thicker electrode. Meanwhile, the Li^+ de-intercalating from the anode flowed through the separator and intercalated in the cathode during the discharging process. Therefore, in the thicker electrode, some part of the Li^+ flowed through a much longer distance, which led to a higher potential drop in the electrode. Because of these two facts, the ohmic heat in the thicker electrode was much higher than that in the thinner electrode.

From the perspective of thermal behavior, an increase in electrode thickness decreases the thermal stability and accelerates the cell degradation rate because of the stronger thermal response and dramatically fluctuating distribution of the heat generation rate in the electrode [34]. First, the higher total heat generation rate in the cell with a thicker electrode resulted in a stronger thermal response and led to the cell operating under deteriorating thermal conditions. This will also decrease the thermal safety, and a more effective thermal management system is required for packs with this type of cells [35, 36]. Second, both the

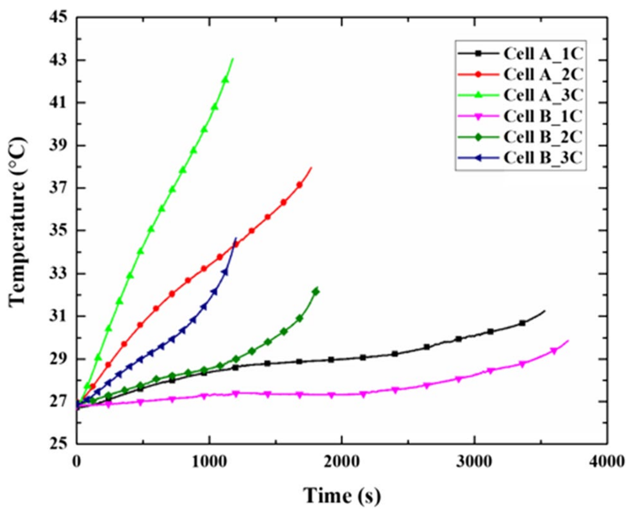

Fig. 10 Average superficial temperature variations of cell-A and cell-B in the experiments

difference in temperature response and uneven heat distribution across the electrode in these two electrodes could lead to a faster degradation rate of the electrode material. Particularly for the distribution of heat generation, as analyzed in Ref. [10], there was a consistent trend between the heat generation rate distribution and local current density across the cell unit, as plotted in Fig. 7, which shows a fluctuating distribution across the cell unit. This was more uneven in the cell with a thicker electrode than in the cell with a thinner electrode. This fluctuating heat generation rate distribution resulted from the coupled effect of non-uniform ohmic heat generation and local current density (Fig. 7), which was directly correlated to the electrochemical heat generation and polarization heat generation [10]. The stronger thermal response for the whole cell and the uneven heat generation distribution were responsible for the faster capacity degradation rate and detachment of the capacity–voltage curves in the long-term cycle tests for the two cells.

In summary, the thickness of the electrode had an obvious influence on the electrochemical characteristics and thermal behavior, as analyzed above. Increasing the thickness of the electrode can effectively improve the energy density and decrease the production cost of commercial large-scale lithium-ion cells because it can save process time for coating, calendering, and cutting for a cell with a specific capacity and simplify the pack structure for the required capacity. However, special attention should be given to the fact that as the electrode thickness increased, the allowable discharging power density of the cell decreased due to the transportation limitations of Li^+ in the thicker electrode; simultaneously, the lifespan also shortened because of the mechanical stress distribution and higher thermal response. Power density, i.e., the allowable maximal discharge rate, is of great importance for hybrid electric vehicle (HEV) and electric vehicle (EV) applications. A trade-off exists between the energy density and power density with a change in the electrode thickness. To achieve a higher energy density, a cell with a thicker electrode can be used at a lower C-rate. For applications requiring a higher power density, decreasing the thickness of the electrode and reducing the energy density from the perspective of the electrode structure would be a suitable method.

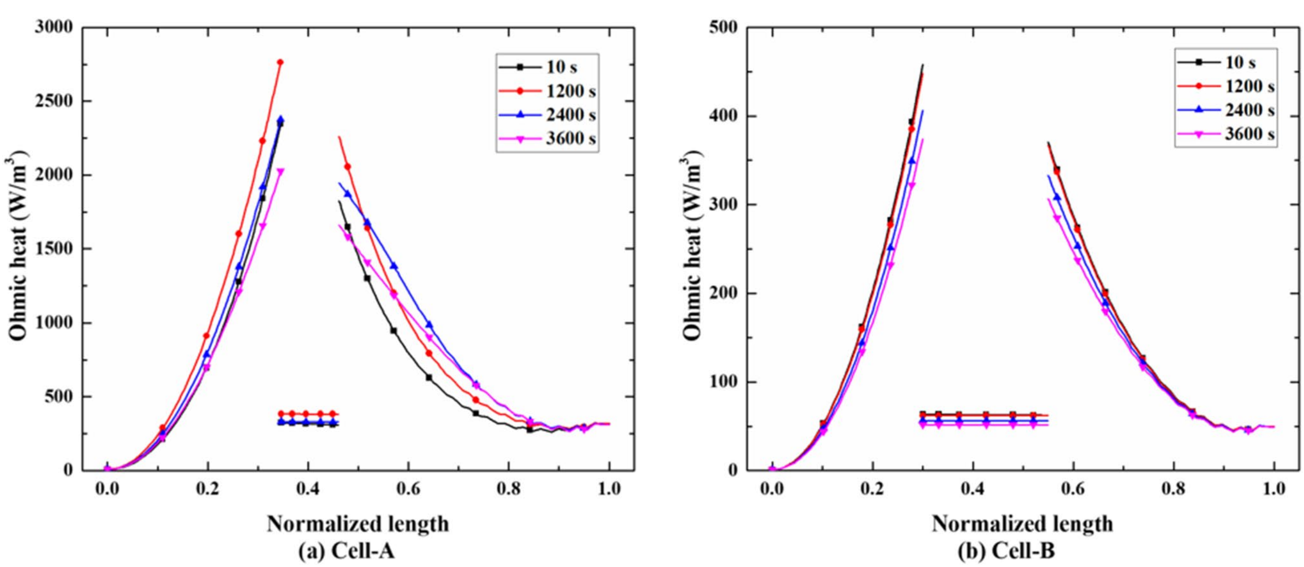

Fig. 11 The ohmic heat generation rate during 1C discharge rate at assigned time point

Conclusions

In the present study, the electrochemical characteristics and thermal behavior of cells with various electrode thicknesses were investigated using experiments and an electrochemical–thermal coupled model. The following conclusions were obtained:

(1) An increase in the electrode thickness improves the energy density because of the reduction in the volume proportion of inactive material in the cell. The detrimental effect of a thicker electrode is a decrease in the power density of the cell owing to the strong transportation limitation of Li^+ in the thicker electrode.
(2) The cell with a thicker electrode showed a lower voltage plateau and an earlier stopping of the discharging process compared with the cell with a thinner electrode. This could be attributed to the larger internal resistance of the cell with the thicker electrode resulting from the longer Li^+ transport pathway and polarization effect.
(3) The cell with a thicker electrode exhibited an intensive thermal response and a non-uniform heat generation rate distribution in the cross-plane direction owing to the higher volumetric proportion of the electrode material, larger internal resistance, and applied current density.
(4) In the long-term cyclic tests, the cell with a thicker electrode presented a faster capacity degradation rate of 0.4 mAh per cycle, whereas the capacity of cell-B remained approximately constant throughout the cyclic process. This could be attributed to a stronger mechanical stress due to the uneven lithiation/delithiation reaction rate as well as the more intensive thermal response.

Funding This work was supported by the project of Natural Science Foundation of Gansu Province (Grant No. 20JR10RA193, Grant No. 18JR3RA141), National Natural Science Foundation of China (Grant No. 51806093), Doctoral Research Funds of Lanzhou University of Technology (Grant No. 061907).

References

1. An Z, Jia L, Ding Y, Dang C, Li X (2017) A review on lithium-ion power battery thermal management technologies and thermal safety. J Therm Sci 26:391–412
2. Men X, Kong X, Yang X, Wang B, Wang Y, Liu Y, Yu L, Li H, Xu B (2020) Synthesis of a pomegranate shaped reduced graphene oxide stabilized secondary Si nanoparticles composite anode for lithium ion batteries. Int J Hydrogen Energy 45:29492–29504
3. Liao Q, Mu M, Zhao S, Zhang L, Jiang T, Ye J, Shen X, Zhou G (2017) Performance assessment and classification of retired lithium ion battery from electric vehicles for energy storage. Int J Hydrogen Energy 42:18817–18823
4. Sakti A, Michalek JJ, Fuchs ERH, Whitacre JF (2015) A techno-economic analysis and optimization of Li-ion batteries for light-duty passenger vehicle electrification. J Power Sources 273:966–980
5. Nam W, Kim J-Y, Oh K-Y (2018) The characterization of dynamic behavior of Li-ion battery packs for enhanced design and states identification. Energy Convers Manage 162:264–275
6. Xu M, Reichman B, Wang X (2019) Modeling the effect of electrode thickness on the performance of lithium-ion batteries with experimental validation. Energy 186:115864
7. Zheng H, Li J, Song X, Liu G, Battaglia VS (2012) A comprehensive understanding of electrode thickness effects on the electrochemical performances of Li-ion battery cathodes. Electrochim Acta 71:258–265
8. Hamankiewicz B, Michalska M, Krajewski M, Ziolkowska D, Lipinska L, Korona K, Kaminska M, Czerwinski A (2014) The effect of electrode thickness on electrochemical performance of $LiMn_2O_4$ cathode synthesized by modified sol–gel method. Solid State Ionics 262:9–13
9. Thunman M, Marquardt K, Hahn R, Kober D, Goerke O, Schubert H (2012) Discharge performance dependence on electrode thickness for Li4Ti5O12LiMn2O4 cells for application in wafer-integrated microbatteries. ECS Trans 41:147–157
10. An Z, Jia L, Wei L, Dang C, Peng Q (2018) Investigation on lithium-ion battery electrochemical and thermal characteristic based on electrochemical-thermal coupled model. Appl Therm Eng 137:792–807
11. Zhang J, Lu B, Song Y, Ji X (2012) Diffusion induced stress in layered Li-ion battery electrode plates. J Power Sources 209:220–227
12. Song Y, Lu B, Ji X, Zhang J (2012) Diffusion induced stresses in cylindrical lithium-ion batteries: analytical solutions and design insights. J Electrochem Soc 159:A2060–A2068
13. Jaguemont J, Boulon L, Dubé Y (2016) A comprehensive review of lithium-ion batteries used in hybrid and electric vehicles at cold temperatures. Appl Energy 164:99–114
14. Xiong R, Li L, Li Z, Yu Q, Mu H (2018) An electrochemical model based degradation state identification method of Lithium-ion battery for all-climate electric vehicles application. Appl Energy 219:264–275
15. Xuefei H, Yingxia H, Huanxin L (2019) Electrochemical-thermal coupled investigation of lithium iron phosphate cell performances under air-cooled conditions. Appl Therm Eng 147:907–916
16. Jiang G, Zhuang L, Hu Q, Liu Z, Huang J (2020) An investigation of heat transfer and capacity fade in a prismatic Li-ion battery based on an electrochemical-thermal coupling model. Applied Thermal Engineering 171:115080
17. Tan M, Gan Y, Liang J, He L, Li Y, Song S, Shi Y (2020) Effect of initial temperature on electrochemical and thermal characteristics of a lithium-ion battery during charging process. Applied Thermal Engineering 177:115500
18. Mei W, Chen H, Sun J, Wang Q (2019) The effect of electrode design parameters on battery performance and optimization of electrode thickness based on the electrochemical–thermal coupling model, Sustainable. Energy Fuels 3:148–165
19. Newman J, Tiedemann W (1975) Porous electrode theory with battery application. AIChE J 21:25–41
20. Rao L, Newman J (1997) Heat-Generation rate and general energy balance for insertion battery systems. J Electrochem Soc 144:2697–2704
21. An Z, Jia L, Wei L, Yang C (2018) Numerical modeling and analysis of thermal behavior and Li+ transport characteristic in lithium-ion battery. Int J Heat Mass Transf 127:1351–1366

22. Jiang F, Peng P, Sun Y (2013) Thermal analyses of $LiFePO_4$/graphite battery discharge processes. J Power Sources 243:181–194
23. Du S, Lai Y, Ai L, Ai L, Cheng Y, Tang Y, Jia M (2017) An investigation of irreversible heat generation in lithium ion batteries based on a thermo-electrochemical coupling method. Appl Therm Eng 121:501–510
24. Zhao R, Liu J, Gu J (2015) The effects of electrode thickness on the electrochemical and thermal characteristics of lithium ion battery. Appl Energy 139:220–229
25. Xu M, Zhang Z, Wang X, Jia L, Yang L (2014) Two-dimensional electrochemical–thermal coupled modeling of cylindrical $LiFePO_4$ batteries. J Power Sources 256:233–243
26. Huang X, Ke S, Lv H, Liu Y (2018) A dynamic capacity fading model with thermal evolution considering variable electrode thickness for lithium-ion batteries. Ionics 24:3439–3450
27. Ogihara N, Itou Y, Sasaki T, Takeuchi Y (2015) Impedance spectroscopy characterization of porous electrodes under different electrode thickness using a symmetric cell for high-performance lithium-ion batteries. The Journal of Physical Chemistry C 119:4612–4619
28. Harris SJ, Timmons A, Baker DR, Monroe C (2010) Direct in situ measurements of Li transport in Li-ion battery negative electrodes. Chem Phys Lett 485:265–274
29. Wu W, Wu W, Qiu X, Wang S (2019) Low-temperature reversible capacity loss and aging mechanism in lithium-ion batteries for different discharge profiles. Int J Energy Res 43:243–253
30. Wu W, Ma R, Liu J, Liu M, Wang W, Wang Q (2021) Impact of low temperature and charge profile on the aging of lithium-ion battery: non-invasive and post-mortem analysis. Int J Heat Mass Tran 170:121024
31. Lin C, Tang A, Mu H, Wang W, Wang C (2015) Aging mechanisms of electrode materials in lithium-ion batteries for electric vehicles. J Chem 2015:1–11
32. Li X, Fang Q, Li J, Wu H, Liu Y, Wen P (2015) Diffusion-induced stress and strain energy affected by dislocation mechanisms in a cylindrical nanoanode. Solid State Ionics 281:21–28
33. Li J, Fang Q, Liu F, Liu Y (2014) Analytical modeling of dislocation effect on diffusion induced stress in a cylindrical lithium ion battery electrode. J Power Sources 272:121–127
34. Valentin O, Thivel P-X, Kareemulla T, Cadiou F, Bultel Y (2017) Modeling of thermo-mechanical stresses in Li-ion battery. Journal of Energy Storage 13:184–192
35. An Z, Jia L, Li X, Ding Y (2017) Experimental investigation on lithium-ion battery thermal management based on flow boiling in mini-channel. Appl Therm Eng 117:534–543
36. Lei Z, Maotao Z, Xiaoming X, Donghai H, Jing W, Renzheng L, Jiaqi F (2018) Heat dissipation analysis of double-layer battery pack under coupling heat transfer of air, liquid, and solid. Int J Energy Res 42:4840–4852